

Barkhausen effect in the first order structural phase transition in type-II Weyl semimetal MoTe₂

Chuanwu Cao^{1,2}, Xin Liu^{1,2}, Xiao Ren^{1,2}, Xianzhe Zeng^{1,2}, Kenan Zhang^{2,3}, Dong Sun^{1,2}, Shuyun Zhou^{2,3}, Yang Wu⁴, Yuan Li^{1,2}, Jian-Hao Chen^{*1,2}

¹International Center for Quantum Materials, School of Physics, Peking University, NO. 5 Yiheyuan Road, Beijing, 100871, China

²Collaborative Innovation Center of Quantum Matter, Beijing 100871, China

³State Key Laboratory of Low Dimensional Quantum Physics, Department of Physics, Tsinghua University, Beijing 100084, China

⁴Tsinghua-Foxconn Nanotechnology Research Center, Tsinghua University, Beijing 100084, China.

E-mail: chenjianhao@pku.edu.cn

Keywords: 2D materials, Barkhausen effect, structural phase transition, MoTe₂

Abstract:

We report the first observation of the non-magnetic Barkhausen effect in van der Waals layered crystals, specifically, between the T_d and $1T'$ phases in type-II Weyl semimetal MoTe₂. Thinning down the MoTe₂ crystal from bulk material to about 25nm results in a drastic strengthening of the hysteresis in the phase transition, with the difference in critical temperature increasing from ~40K to more than 300K. The Barkhausen effect appears for thin samples and the temperature range of the Barkhausen zone grows approximately linearly with reducing sample thickness, pointing to a surface origin of the phase pinning defects. The distribution of the Barkhausen jumps shows a power law behavior, with its critical exponent $\alpha = 1.27$, in good agreement with existing scaling theory. Temperature-dependent Raman spectroscopy on MoTe₂ crystals of various thicknesses shows results consistent with our transport measurements.

Introduction

Layered transition metal dichalcogenides (TMDs), a family of van der Waals crystals, have attracted extensive research interests due to their intriguing properties[1-4]. Certain TMDs have rich structural and electronic phases which exhibit drastically different physical properties[5-15]. MoTe₂, in particular, is an excellent example of such multi-phase materials, which possesses three different crystal structures: hexagonal $2H$, monoclinic $1T'$, and orthorhombic T_d [14]. The $2H$ phase MoTe₂ is a semiconductor and candidate material for two-dimensional field effect transistors (2D-FET)[16]. The $1T'$ phase MoTe₂ is a quantum spin Hall candidate at the single layer form [17,18], and a central symmetric semimetal at the multi-layer form, whose crystal symmetry belongs to the $P2_1/m$ space group [14]. The non-centrosymmetric T_d phase MoTe₂ belongs to the $Pmn2_1$ space group and is a type-II Weyl semimetal which violates the Lorentz invariant, with the Weyl points appear as the touching points between electron and hole pocket in a tiled cone configuration[14,15].

The structural phase transition of MoTe₂ between the $1T'$ phase and the $2H$ phase can be achieved by electrostatic gating at room temperature [8], while the transition between the $1T'$ phase and the T_d phase can be achieved by varying the sample temperature[14]. The temperature driven structural phase transition between T_d (low temperature phase) and $1T'$ (high temperature phase) has been demonstrated by electrical transport[19, 20], Raman spectroscopy [14] and angle-resolved photoemission spectroscopy [15]. In this article, we report the first observation of Barkhausen physics in the first order structural phase transition between the two metallic phases of MoTe₂ (the $1T'$ phase and the T_d phase).

The Barkhausen effect is originally defined as a series of sudden reversal of Weiss domains in a ferromagnet during a continuous process of magnetization or demagnetization[21-23]. The Barkhausen physics is related to domain-wall pinning and de-pinning when a ferromagnetic system experiences a transition between two different states. During the transition, the domain wall between two states moves through the sample. Defects in the crystal pin the moving domain wall and hold the neighbor area in the past state until the energy gain in flipping the whole neighbor area

gets larger than the de-pinning energy. When de-pinning happens, the pinned area suddenly turns into the other state, leading to a jump in the total magnetization of the sample (see supplementary materials figure S1). The Barkhausen effect has been a powerful tool to characterize magnetic and ferroelectric materials[24-27], and it has also attracted growing interest as an example of complex dynamical systems displaying dimension-dependent scaling behavior [22]. Given the ubiquitous presence of the Barkhausen effect in magnetic phase transition[24-29], only a limited number of research has revealed Barkhausen physics in thermally-driven first-order phase transition in non-magnetic materials[30-35], and none of such transition has been observed in van der Waals layered crystals.

Here, we report the first observation of the thickness-dependent Barkhausen effect in the thermally-driven first order structural phase transition between the T_d phase and the $1T'$ phase in MoTe_2 . The T_d phase and $1T'$ phase MoTe_2 are both metallic but with different resistivity at any given temperature (e.g. $\rho_{T_d} < \rho_{1T'}$). Thus, careful measurement of the resistivity of the MoTe_2 as a function of temperature $\rho(T)$ reveals events of the structural phase transition in the crystal.

For bulk crystals, the phase transition happens sharply at around 250K with no additional features, and hysteresis of the transition temperature, defined as $T_{\text{hysteresis}} = T_{T_d \rightarrow 1T'} - T_{1T' \rightarrow T_d}$, is around 40K (figure 1b). For samples between 100nm-20nm, on the other hand, the phase transition occurs in a large temperature region and exhibits a series of kinks in $\rho(T)$, which is a manifestation of the Barkhausen effect. Thinning down the MoTe_2 crystal from bulk material to about 20nm results in a drastic strengthening of the hysteresis in the phase transition, with $T_{\text{hysteresis}}$ increasing from ~40K to more than 300K. The temperature range of the Barkhausen zone grows approximately linearly with reducing sample thickness as determined by four-probe resistivity measurement. The distribution of the Barkhausen jumps shows a power law behavior, with its critical exponent $\alpha = 1.27$, consistent with theoretical expectations as explained later in this letter. Temperature-dependent Raman spectroscopy is also performed on MoTe_2 crystals of various thicknesses, showing results consistent with our transport measurements.

Results and discussion

The temperature-driven structural phase transition in few-layer metallic MoTe₂ is studied using electrical transport measurement as well as Raman spectroscopy. Figure 1a shows the atomic schematics of MoTe₂ in T_d phase and in $1T'$ phase. The T_d phase MoTe₂ shares the same in-plane crystal structure with the $1T'$ phase MoTe₂ and differs only in vertical stacking[14]. Figure 1b shows a typical temperature-dependent four-probe resistivity curve of bulk metallic MoTe₂. The transition from $1T'$ phase to T_d phase occurs at about 230K to 250K and the transition from T_d phase to $1T'$ phase occurs at about 260K to 270K. It is experimentally observed that $\rho_{T_d} < \rho_{1T'}$ at the phase transition temperature, thus $\Delta\rho_{T_d \rightarrow 1T'} > 0$ and $\Delta\rho_{1T' \rightarrow T_d} < 0$.

Figure 1c shows a typical temperature-dependent four-probe resistivity curve $\rho(T)$ for a 50nm-thick MoTe₂ sample, which is fairly different from that of the bulk samples. The cooling curve and warming curve do not overlap from 80K to 320K, showing that the hysteresis of transition between the $1T'$ phase and the T_d phase has been strengthened. While bulk crystals show a smooth function of $\rho(T)$ during the phase transition, a series of kinks in $\rho(T)$ appear in a wide temperature range for both the warming and cooling curves in thinner samples. Here a kink means an instance of rapid change in the $\rho(T)$ curve. We found that all the kinks in the cooling curve ($1T' \rightarrow T_d$, upper inset in figure 1c) represent rapid drops in the resistivity, while all the kinks in the warming curve ($T_d \rightarrow 1T'$, lower inset in figure 1c) represent rapid increase in the resistivity, consistent with the fact that $\Delta\rho_{1T' \rightarrow T_d} < 0$ and $\Delta\rho_{T_d \rightarrow 1T'} > 0$. Thus, both the kinks and the strengthened hysteresis behavior in the $\rho(T)$ curves can be attributed to modified structural phase transition in thin MoTe₂ crystals. The appearance of kinks in the $\rho(T)$ curves reveals the existence of phase pinning in the first order phase transition process in thin MoTe₂. During cooling (warming) process, defects or local strains in the crystal pin their neighbor area in the $1T'$ (T_d) phase; as the temperature becomes sufficiently low (high), the pinned area suddenly flips to the T_d ($1T'$) phase, and be detected as a kink in the $\rho(T)$ curves.

Figure 2a shows $\rho(T)$ curves for seven temperature scans of a 50nm MoTe₂ sample between 10 K and 350K (curves offset for clarity). All the curves show metallic and hysteresis behavior. We found that kinks in the $\rho(T)$ curves do not happen at the same temperature during different experimental runs for the same device, but rather, has a statistical distribution, which is analogous to the Barkhausen effect observed in magnetic materials (e.g. jumps in the $M(H)$ curves has a statistical distribution)[24, 25]. The distribution of the kinks can be summarized as a histogram of the occurrence of the kinks weighted by the height ($\Delta\rho$) of respective kinks, as shown in figure 2b. We collect kinks from all 7 runs of cooling and warming process, sum up all kinks' height in each bin (5K in temperature), and plot the value (in units of Ohms) as a function of temperature. The height of a kink is obtained using a procedure shown in the inset of figure 2a. It is worth pointing out that the kink histogram may not show the full scale of the phase transition, but rather, show the temperature distribution of all the detected Barkhausen jumps. Nonetheless, the kink histogram reveals the temperature range that phase transition occurs. In figure 2b, the blue histogram is extracted from cooling curves, and red from warming curves. Comparing with the bulk, the temperature range of the phase transition shifts and expands to 180K-50K for the $1T' \rightarrow T_d$ transition, and 230K-320K for the $T_d \rightarrow 1T'$ transition. The expansion of $T_{hysteresis}$ can also be explained by the Barkhausen effect, as defects pinning impedes the phase transition process, leading to super-cooled /super-heated states. We notice that the total-height of the Barkhausen jumps in cooling is much larger than in warming. One possible explanation is that the pinning effect is stronger as thermal fluctuation is smaller in lower temperature, thus larger Barkhausen jumps are recorded during cooling than during warming.

To study the evolution of the phase transition temperature as a function of sample thickness, we fabricated several devices with thickness ranging from 6nm to 120nm. For samples between 20nm-100nm, the Barkhausen effect can be observed. We can define the “Barkhausen zone” as the range of temperature between the highest and the lowest kink temperature. For samples thicker than 100nm, Barkhausen jumps disappear and the $\rho(T)$ curves show bulk-like behavior with a shift of

the transition temperature (see supplementary materials figure S2). Figure 3 plots the temperature ranges of the Barkhausen jumps versus sample thickness together with the phase transition temperature range for bulk crystals. The temperature ranges are plotted by dash bars for each thickness. We find that both the upper bound and the lower bound of Barkhausen zone extend approximately linearly when sample thickness is reduced. This phenomenon infers that the pinning effect enhances linearly when sample's layer number decreases, suggesting a possible surface origin of the pinning defects. No transition signal is observed for samples at or below 6nm (see supplementary materials figure S4). Since $1T^p$ and T_d MoTe₂ share the same in-plane structure[14], the phase transition behavior towards the monolayer limit warrants further investigation.

Figure 4 plots the histogram of the normalized resistivity kink height ($\Delta R/R$) for all the devices measured. Here $\Delta R = R_{1T^p} - R_{T_d}$ represents $\sim 5\%$ of the total resistivity of the sample, thus we can assign the total resistivity of the sample $R = R_{1T^p} \cong R_{T_d}$. We found that the distribution function f of $\Delta R/R$ from all the devices we measured follows a power law $f \sim (\Delta R/R)^{-\alpha}$, with $\alpha = 1.27 \pm 0.08$. Theoretically, it has been predicted that the domain size (s) of each Barkhausen jump has a distribution P that follows a power law $P(s) \sim s^{-\beta}$ [22, 23, 28]. Mean-field theory gives a universal exponent $\beta = 2 - 2/(d + 1)$ for such power law behavior, where $d \leq 3$ is the dimension of the system[23]. It is reasonable to assume that ΔR is proportional to the total resistivity R for a given size of flipped domain at any given temperature, thus the size of the flipped domain $s \sim \Delta R/R$. If the Barkhausen effect in thin MoTe₂ is three-dimensional, then $\beta = 1.5$, which does not agree with our experimental observation. On the other hand, if there are mainly two-dimensional phase pinning/depinning in thin MoTe₂, then $\beta = 4/3 \approx 1.33$, which agrees well with the experimentally extracted value of α . This result suggests that the phase transition between $1T^p$ and T_d in thin MoTe₂ could be a rare example for non-magnetic Barkhausen effect in the two dimensional universality class. It is worth noting that the theories describing scaling behavior in a Barkhausen process in magnetic materials is far from united, much less is known for Barkhausen process in non-magnetic structural phase transition. For example, an elastic interface theory predicts

$\beta \approx 1.3$ for a three dimensional Barkhausen process[23, 36, 37]. Thus more theoretical study is needed to fully understand our experimental observation.

As a further verification of the shifting and expansion of the phase transition temperature, we performed temperature-dependent polarized Raman spectroscopy on thin MoTe₂ samples. The strongest Raman signal that distinguishes the $1T'$ and the T_d phases is the interlayer shear mode at $\sim 13\text{cm}^{-1}$, as measured in the parallel-polarized configuration [14]. Centrosymmetry breaking in the T_d structure leads to a Raman active mode at 13cm^{-1} (denoted as the A peak), whereas this mode is Raman inactive in $1T'$ MoTe₂. Figure 5a shows the Raman spectra between 6cm^{-1} and 20cm^{-1} of a 22nm-thick MoTe₂ sample at different temperature during sample cooling (left panel) and warming (right panel). The temperature-dependent evolution of the intensity of the A peak is shown in figure 5b. One can find that the intensity of the peak increases between 235K and 130K during sample cooling, and starts to decrease above 280K during sample warming. Up to 350K, the A peak is still observable for the 22nm sample. This is in stark contrast to bulk MoTe₂, where such change in the intensity of the A peak is completed within 215K to 280K[14]. Figure 5c is the temperature-dependent Raman spectra of a 155nm-thick MoTe₂ sample between 6cm^{-1} and 20cm^{-1} , which shows intermediate behavior between bulk and the 22nm-thick MoTe₂. The observation in figure 5 is consistent with resistivity measurement, showing enhancing $T_{\text{hysteresis}}$ with samples of reducing thickness.

Conclusions

We report the first observation of the Barkhausen effect in the first order structural phase transition between the two metallic phases, e.g., the $1T'$ phase and the T_d phase, of MoTe₂ thin flakes. The temperature range of the Barkhausen zone increase linearly with reducing thickness, pointing to a surface origin of the phase pinning defects. The distribution of normalized resistivity jumps ($\Delta R/R$) has a power law dependence with exponent $\alpha = 1.27 \pm 0.08$, suggesting an underlying scaling behavior. Temperature-dependent Raman spectroscopy also detects thickness

dependent temperature ranges for the phase transition, consistent with data from transport measurement.

Methods

The bulk 1T' MoTe₂ crystals were synthesized by chemical vapor transport method [15, 38-42], and few-layer samples were mechanical exfoliated from bulk crystals and deposited onto silicon wafer with 300nm SiO₂. Standard electron beam lithography and metallization processes were performed to pattern multiple electrodes on few-layer MoTe₂ devices for four-probe measurements. The electrodes were made of 5nm Cr/ 50nm Au. Resistivity measurements were performed in PPMS with lock-in amplifiers. Speed of temperature sweep in the resistivity measurement is 5K/min. Higher and lower sweeping speeds are performed to confirm full thermalization of the sample during the measurement. Raman measurements were performed on exfoliated few-layer MoTe₂ in a confocal back-scattering geometry using a Horiba Jobin Yvon LabRAM HR Evolution spectrometer, equipped with 1800 gr/mm gratings and a liquid-nitrogen-cooled CCD. We used the $\lambda = 514$ nm line of an Argon laser for excitation. The BraggGrate notch filters allow for measurements at low wave numbers. Polarized Raman spectra were measured in a-a configuration.

Acknowledgments

This project has been supported by the National Basic Research Program of China (Grant Nos. 2014CB920900, 2018YFA0305604), and the National Natural Science Foundation of China (Grant Nos.11774010 (C. Cao, X. Liu and J.-H. Chen)) (Grant Nos. 11674013,11704012 (D. Sun)). Crystal drawings were produced by VESTA[43,44].

References

1. Radisavljevic B, Radenovic A, Brivio J, Giacometti V, Kis A. Single-layer MoS₂ transistors. *Nat Nanotechnol.* 2011;6(3):147-50.
2. Wu S, Fatemi V, Gibson QD, Watanabe K, Taniguchi T, Cava RJ, et al. Observation of the quantum spin Hall effect up to 100 Kelvin in a monolayer crystal. *Science.* 2018;359(6371):76-9.
3. Voiry D, Yamaguchi H, Li JW, Silva R, Alves DCB, Fujita T, et al. Enhanced catalytic activity in strained chemically exfoliated WS₂ nanosheets for hydrogen evolution. *Nature Materials.* 2013;12(9):850-5.
4. Zheng F, Cai C, Ge S, Zhang X, Liu X, Lu H, et al. On the Quantum Spin Hall Gap of Monolayer 1T'-WTe₂. *Adv Mater.* 2016;28(24):4845-51.
5. Pan XC, Chen X, Liu H, Feng Y, Wei Z, Zhou Y, et al. Pressure-driven dome-shaped superconductivity and electronic structural evolution in tungsten ditelluride. *Nat Commun.* 2015;6:7805.
6. Yu Y, Yang F, Lu XF, Yan YJ, Cho YH, Ma L, et al. Gate-tunable phase transitions in thin flakes of 1T-TaS₂. *Nat Nanotechnol.* 2015;10(3):270-6.
7. Liu Y, Gu Q, Peng Y, Qi S, Zhang N, Zhang Y, et al. Raman Signatures of Broken Inversion Symmetry and In-Plane Anisotropy in Type-II Weyl Semimetal Candidate TaIrTe₄. *Adv Mater.* 2018;30(25):1706402.
8. Wang Y, Xiao J, Zhu H, Li Y, Alsaïd Y, Fong KY, et al. Structural phase transition in monolayer MoTe₂ driven by electrostatic doping. *Nature (UK).* 2017;550(7677):487-91.
9. Hwang J, Zhang C, Cho K. Structural and electronic phase transitions of MoTe₂ induced by Li ionic gating. *2D Materials.* 2017;4(4):045012.
10. Kim H-J, Kang S-H, Hamada I, Son Y-W. Origins of the structural phase transitions in MoTe₂ and WTe₂. *Phys Rev B.* 2017;95(18):180101.

11. Ueno K, Fukushima K. Changes in structure and chemical composition of α -MoTe₂ and β -MoTe₂ during heating in vacuum conditions. *Applied Physics Express*. 2015;8(9):095201.
12. Cho S, Kim S, Kim JH, Zhao J, Seok J, Keum DH, et al. Phase patterning for ohmic homojunction contact in MoTe₂. *Science*. 2015;349(6248):625-8.
13. Lai J, Liu Y, Ma J, Zhuo X, Peng Y, Lu W, et al. Broadband Anisotropic Photoresponse of the "Hydrogen Atom" Version Type-II Weyl Semimetal Candidate TaIrTe₄. *ACS Nano*. 2018;12(4):4055-61.
14. Zhang K, Bao C, Gu Q, Ren X, Zhang H, Deng K, et al. Raman signatures of inversion symmetry breaking and structural phase transition in type-II Weyl semimetal MoTe₂. *Nat Commun*. 2016;7:13552.
15. Deng K, Wan G, Deng P, Zhang K, Ding S, Wang E, et al. Experimental observation of topological Fermi arcs in type-II Weyl semimetal MoTe₂. *Nature Physics*. 2016;12(12):1105-10.
16. Larentis S, Fallahazad B, Movva HCP, Kim K, Rai A, Taniguchi T, et al. Reconfigurable Complementary Monolayer MoTe₂ Field-Effect Transistors for Integrated Circuits. *ACS Nano*. 2017;11(5):4832-9.
17. Qian X, Liu J, Fu L, Li J. Quantum spin Hall effect in two-dimensional transition metal dichalcogenides. *Science*. 2014;346(6215):1344-7.
18. Nie SM, Song Z, Weng H, Fang Z. Quantum spin Hall effect in two-dimensional transition-metal dichalcogenide haeckelites. *Phys Rev B*. 2015;91(23):235434.
19. Hughes H, Friend R. Electrical resistivity anomaly in β -MoTe₂ (metallic behaviour). *Journal of Physics C: Solid State Physics*. 1978;11(3):L103.
20. He R, Zhong S, Kim HH, Ye G, Ye Z, Winford L, et al. Dimensionality-driven orthorhombic MoTe₂ at room temperature. *Phys Rev B*. 2018;97(4):041410.

21. Barkhausen H. Zwei mit Hilfe der neuen Verstärker entdeckte Erscheinungen. *Phys Z.* 1919;20:401.
22. Alessandro B, Beatrice C, Bertotti G, Montorsi A. Domain-wall dynamics and barkhausen effect in metallic ferromagnetic materials .1. Theory. *J Appl Phys.* 1990;68(6):2901-7.
23. Zapperi S, Cizeau P, Durin G, Stanley HE. Dynamics of a ferromagnetic domain wall: Avalanches, depinning transition, and the Barkhausen effect. *Phys Rev B, Condens Matter (USA).* 1998;58(10):6353-66.
24. Sethna JP, Dahmen KA, Myers CR. Crackling noise. *Nature (UK).* 2001;410(6825):242-50.
25. Spasojevic D, Bukvic S, Milosevic S, Stanley HE. Barkhausen noise: Elementary signals, power laws, and scaling relations. *Phys Rev E.* 1996;54(3):2531-46.
26. Das P, Porrati F, Wirth S, Bajpai A, Huth M, Ohno Y, et al. Magnetization dynamics of a CrO₂ grain studied by micro-Hall magnetometry. *Applied Physics Letters.* 2010;97(4):089902.
27. Chynoweth AG. Barkhausen pluses in barium titanate. *Phys Rev.* 1958;110(6):1316-32.
28. Durin G, Zapperi S. Scaling exponents for Barkhausen avalanches in polycrystalline and amorphous ferromagnets. *Phys Rev Lett.* 2000;84(20):4705-8.
29. Chizhik A, Stupakiewicz A, Maziewski A, Zhukov A, Gonzalez J, Blanco J. Direct observation of giant Barkhausen jumps in magnetic microwires. *Applied Physics Letters.* 2010;97(1):012502.
30. Mai MF, Kliem H. Observation of thermal Barkhausen effect in ferroelectric films of poly(vinylidene fluoride/trifluoroethylene) copolymer. *J Appl Phys.* 2013;114(22):224104.
31. Huber-Rodriguez B, Kwang SY, Hardy WJ, Ji H, Chen CW, Morosan E, et al. Thermally driven analog of the Barkhausen effect at the metal-insulator transition in vanadium dioxide. *Applied Physics Letters.* 2014;105(13):131902.

32. Yu GQ, Ren C, Rizwan S, Yu T, Xu K, Han XF. Superconductivity-induced pinning effect in superconductor/magnetic tunnel junctions. *Spin*. 2013;3(1):1350006.
33. Garcia-Fornaris I, Govea-Alcaide E, Alberteris-Campos M, Mune P, Jardim RF. Transport Barkhausen-like noise in uniaxially pressed $\text{Bi}_{1.65}\text{Pb}_{0.35}\text{Sr}_2\text{Ca}_2\text{Cu}_3\text{O}_{10+\delta}$ ceramic samples. *Physica C*. 2010;470(15-16):611-6.
34. Mazzetti P, Stepanescu A, Tura P, Masoero A, Puica I. Barkhausen-like conductance noise in polycrystalline high- T_c superconductors immersed in a slowly varying magnetic field. *Phys Rev B*. 2002;65(13):132512.
35. Perez-Reche FJ, Tadic B, Manosa L, Planes A, Vives E. Driving rate effects in avalanche-mediated first-order phase transitions. *Phys Rev Lett*. 2004;93(19):195701.
36. Narayan O, Fisher DS. Threshold critical dynamics of driven interfaces in random media. *Phys Rev B*. 1993;48(10):7030-42.
37. Leschhorn H, Nattermann T, Stepanow S, Tang LH. Driven interface depinning in a disordered medium. *Ann. Phys.-Leip*. 1997;6(1):1-34.
38. Keum DH, Cho S, Kim JH, Choe D-H, Sung H-J, Kan M, et al. Bandgap opening in few-layered monoclinic MoTe_2 . *Nature Physics*. 2015;11(6):482-6.
39. Pradhan NR, Rhodes D, Feng S, Xin Y, Memaran S, Moon B-H, et al. Field-Effect Transistors Based on Few-Layered α - MoTe_2 . *ACS Nano*. 2014;8(6):5911-20.
40. Naylor CH, Parkin WM, Ping J, Gao Z, Zhou YR, Kim Y, et al. Monolayer Single-Crystal $1T'$ - MoTe_2 Grown by Chemical Vapor Deposition Exhibits Weak Antilocalization Effect. *Nano Lett*. 2016;16(7):4297-304.
41. Yamamoto M, Wang ST, Ni MY, Lin YF, Li SL, Aikawa S, et al. Strong Enhancement of Raman Scattering from a Bulk-Inactive Vibrational Mode in Few-Layer MoTe_2 . *ACS Nano*. 2014;8(4):3895-903.
42. Qi Y, Naumov PG, Ali MN, Rajamathi CR, Schnelle W, Barkalov O, et al. Superconductivity in Weyl semimetal candidate MoTe_2 . *Nat Commun*. 2016;7:11038.

43. Momma K, Izumi F. VESTA 3 for three-dimensional visualization of crystal, volumetric and morphology data. *Journal of applied crystallography*. 2011;44(6):1272-6.
44. *Acta Crystallographica* (1,1948-23,1967) (1966) 20, p268-p274.

Figure 1

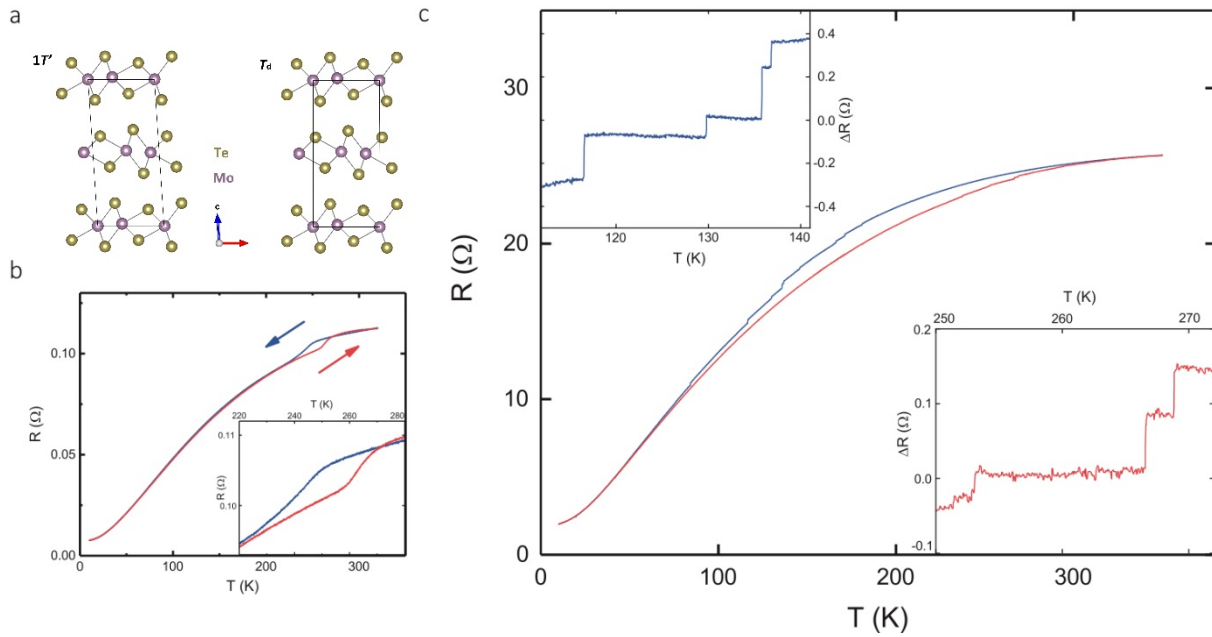
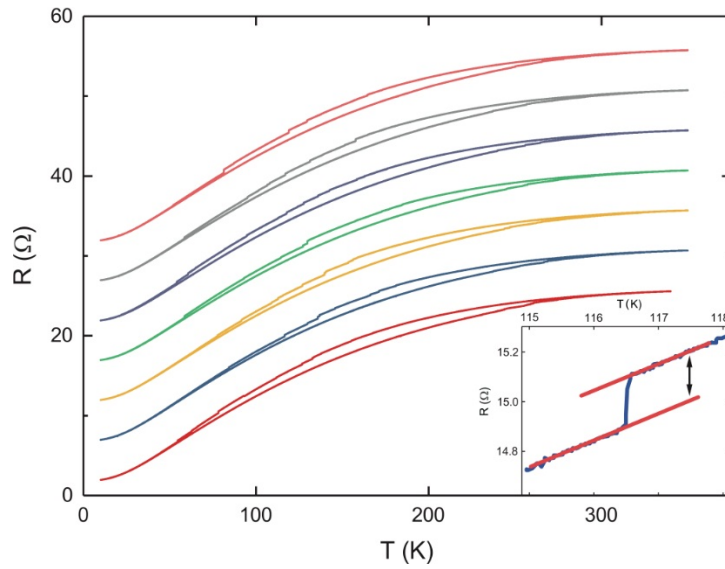


Fig1: **Temperature-induced phase transition in few-layer MoTe_2 .**

- (a) Crystal structures of $1T'$ and T_d phase MoTe_2 .
- (b) Temperature dependent resistivity of a bulk MoTe_2 sample; cooling curve in blue, warming in red.
- (c) Temperature dependent resistivity of a 50nm MoTe_2 sample. Cooling curve in blue, warming in red. Upper (lower) insets: zoom-in of the cooling (warming) curve in (c) with background subtracted.

Figure 2

a



b

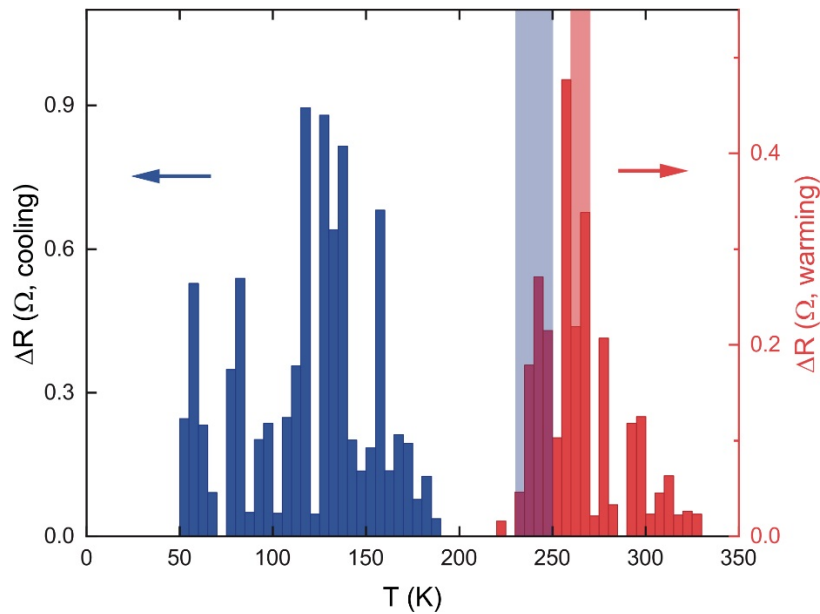


Fig2: Barkhausen jumps in few-layer MoTe₂.

- (a) Repeated temperature dependent resistivity measurement of the 50nm MoTe₂ sample. Seven runs of the cooling-warming process are plotted together with Y-offset. The inset shows the method to determine kink height.
- (b) Histogram of resistivity kinks in figure 2a, weighted by kink's height. Kinks in cooling and warming are plotted side-by-side. Blue- and red-shaded area is the phase transition region for bulk MoTe₂ crystals during cooling and warming, respectively.

Figure 3

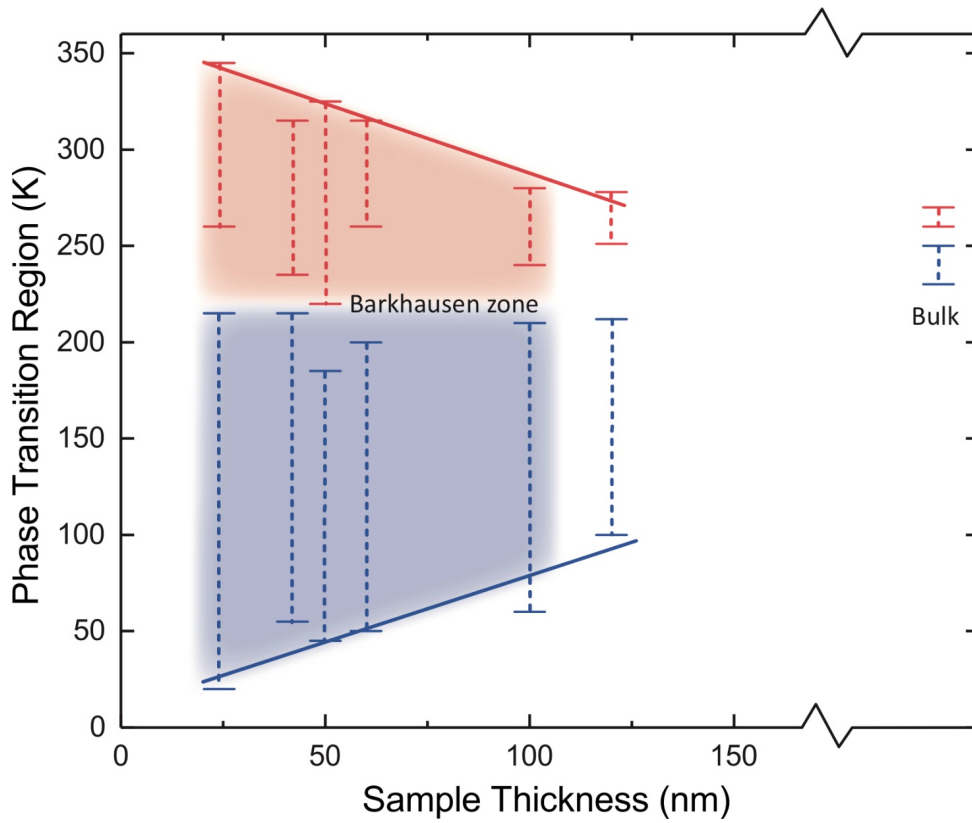


Fig3: **Thickness dependent phase transition temperature ranges.**

Barkhausen zone as a function of sample thickness. Barkhausen zone is extracted by the highest/lowest temperature that Barkhausen jumps appear, and are plotted by blue bars and red bars for cooling and warming, respectively. Shaded area denotes the parameter space of temperature and sample thickness where Barkhausen effect is detected. For sample thicker than 100nm, the endpoints are determined by the temperature at which cooling and warming curves begins to overlap.

Figure 4

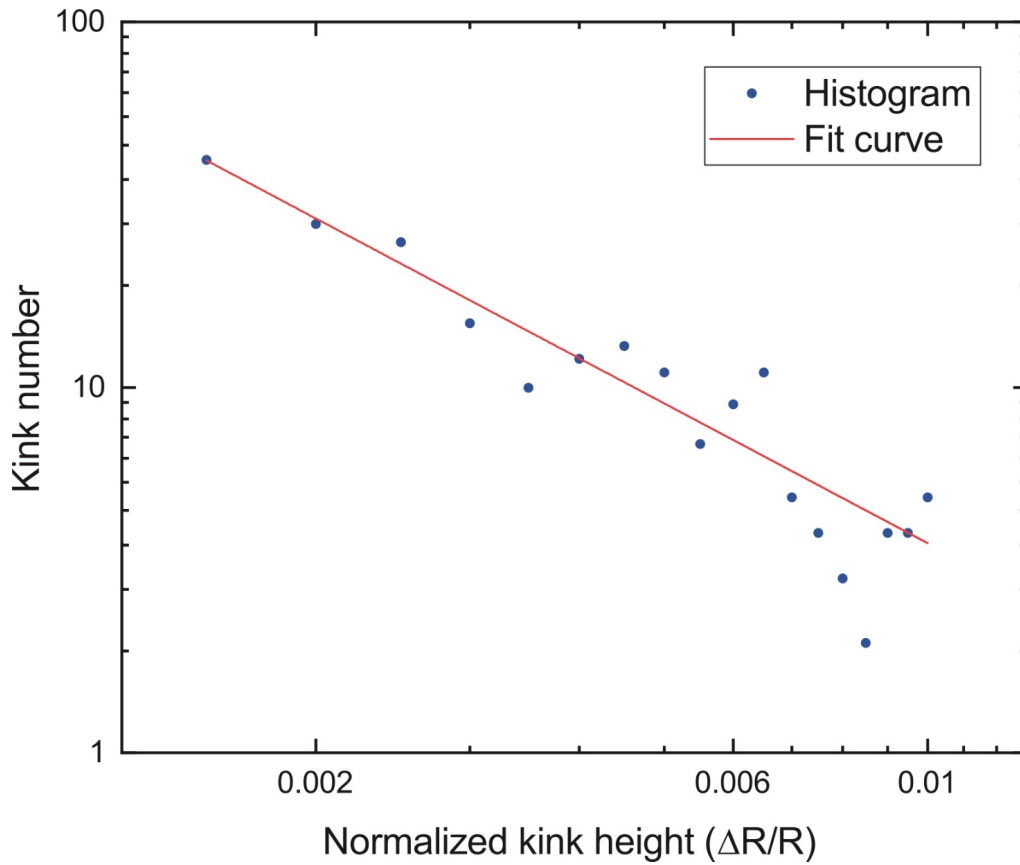


Fig4: **Distribution of normalized resistivity kink height.**

Histogram of normalized resistivity kink height $\Delta R/R$ for all the samples (blue dots), where R is the sample resistivity at the resistivity jump, and ΔR is the respective jumps in resistivity. Red line shows a power law fitting. Exponent $\alpha = 1.27 \pm 0.08$ is obtained from the fit.

Figure 5

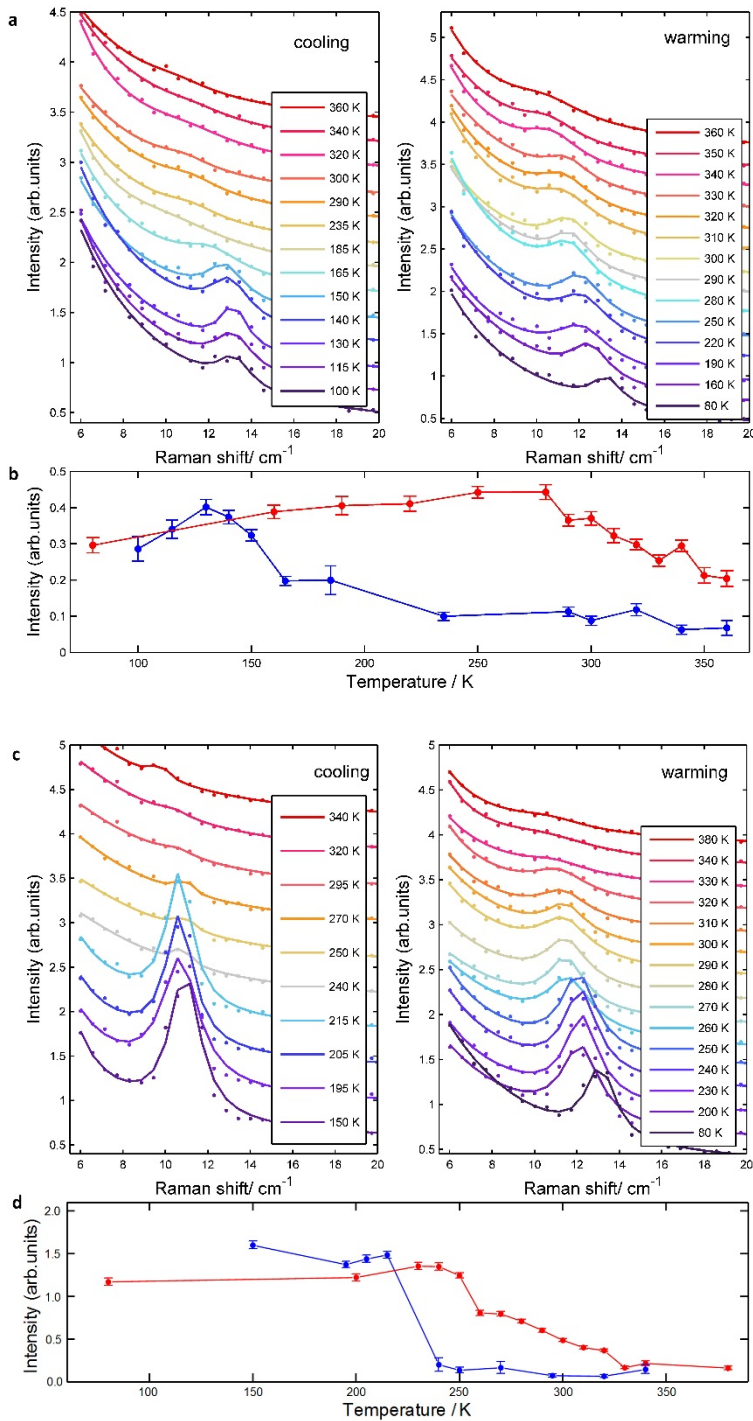


Fig5: Temperature dependence of polarized Raman spectra for the signal at 13 cm^{-1} . Temperature dependent Raman spectra around 13 cm^{-1} for (a) a 22nm sample, (c) a 155 nm sample. Temperature dependence of the Raman intensity for the 13 cm^{-1} peak for (b) a 22nm sample, (d) a 155 nm sample. Blue for cooling and red for warming in (b) and (d).

Supplementary materials

Figure.S1 to Figure.S5

Figure S1

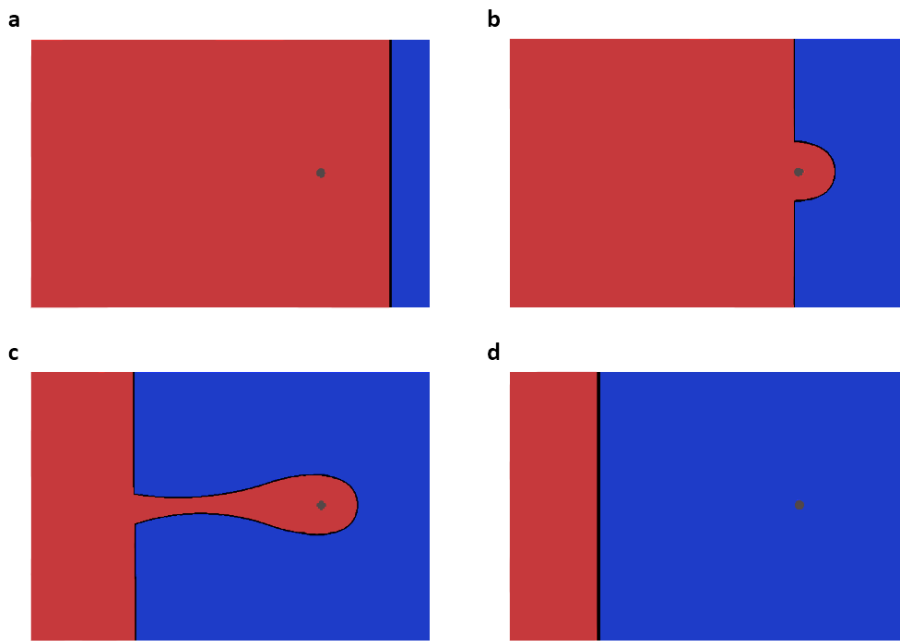


Fig.S1: 2D Schematic for the Barkhausen effect.

Phase transition with Barkhausen effect is shown in time order: (a) \rightarrow (b) \rightarrow (c) \rightarrow (d). Blue and red area stands for two different states. The pinning defect is plotted as a gray dot. During the transition, the domain wall move through the defect, which pins its neighbor area in the past state (b,c). When de-pinning happens (d), the pinned area suddenly turns into the other state, which can be observed as a Barkhausen jump.

Figure S2

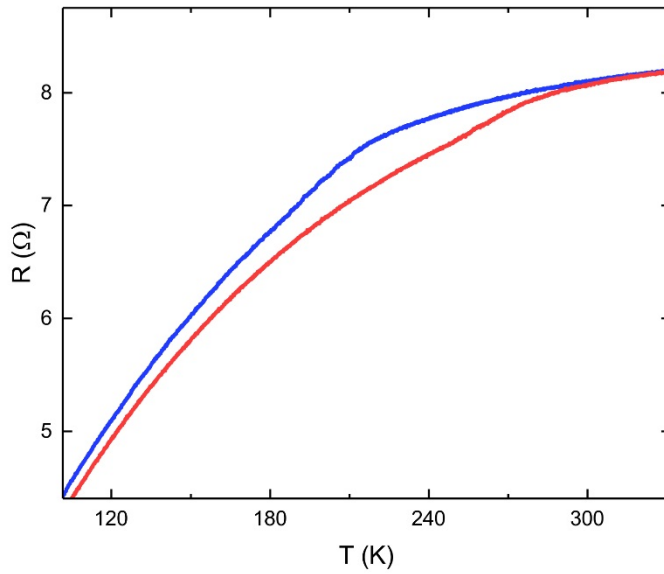


Fig.S2: **Resistivity of few-layer MoTe₂ out of the Barkhausen zone.**

Four-probe resistivity measurement of a 120nm MoTe₂ sample. Barkhausen jump disappear and normal phase transition curve remains. The transition appears at 200K and 250K for cooling and warming, respectively. Phase transition temperate is different from bulk behavior as shown in figure 1b.

Figure S3

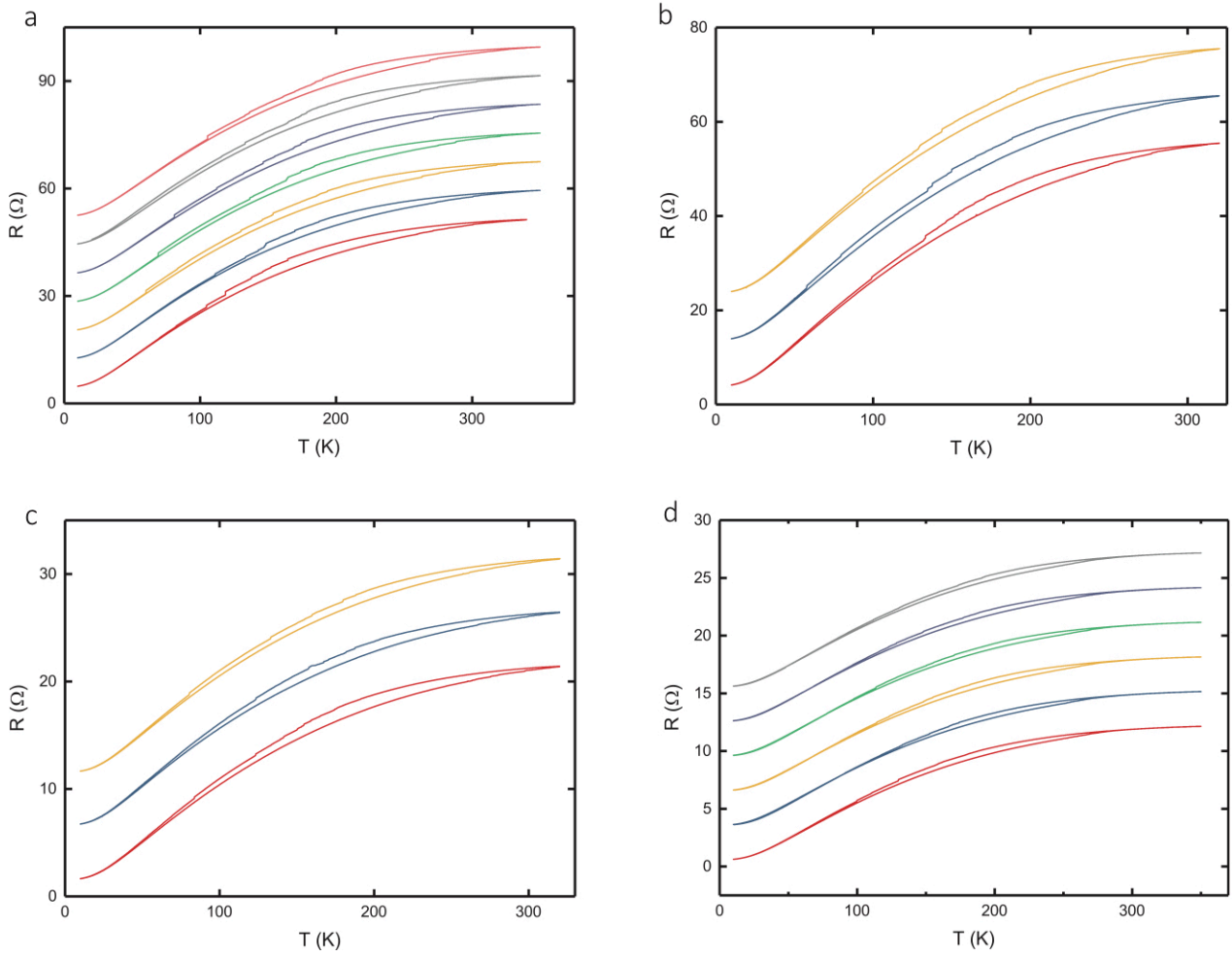


Fig.S3: **Barkhausen jumps in various few-layer MoTe_2 devices.**

Four-probe resistivity measurement of few-layer MoTe_2 samples with different thickness. Several runs of cooling-warming curves are plotted together with Y-offset. All the curves show resistivity kinks in a large temperature range. Sample thickness are (a) 24nm, (b) 42nm, (c) 60nm, and (d) 100nm, respectively.

Figure S4

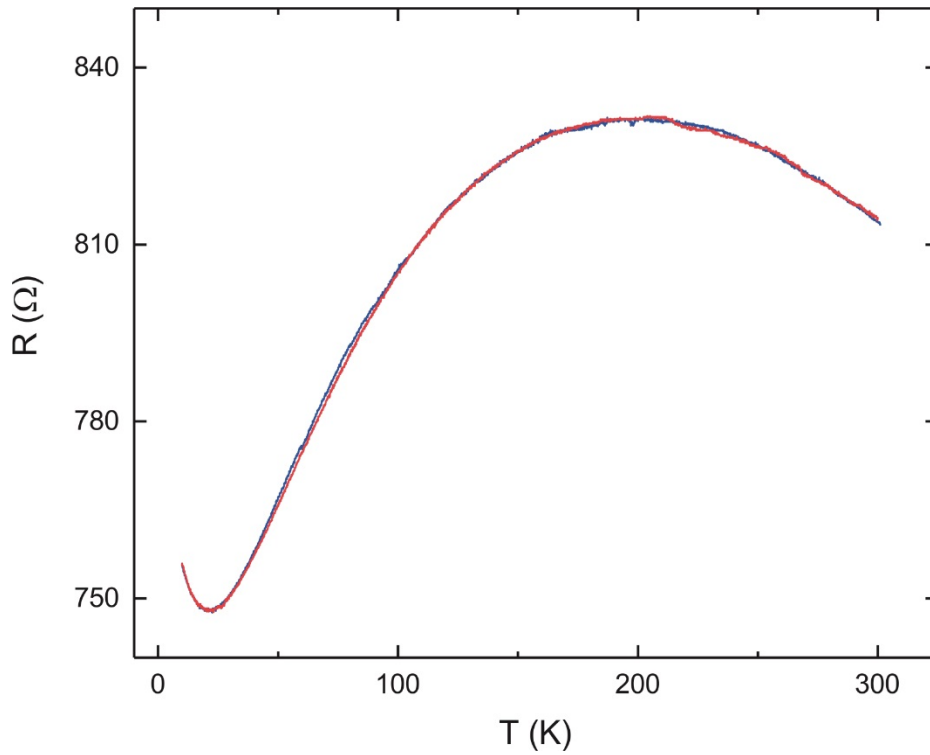


Fig.S4: **Resistivity of a 6nm MoTe₂ device.**

Four-probe resistivity measurement of a 6nm MoTe₂ sample. The cooling (blue) and warming (red) curve overlap from 300K to 10K. No structural phase transition signal is observed from electrical transport measurement.

Figure S5

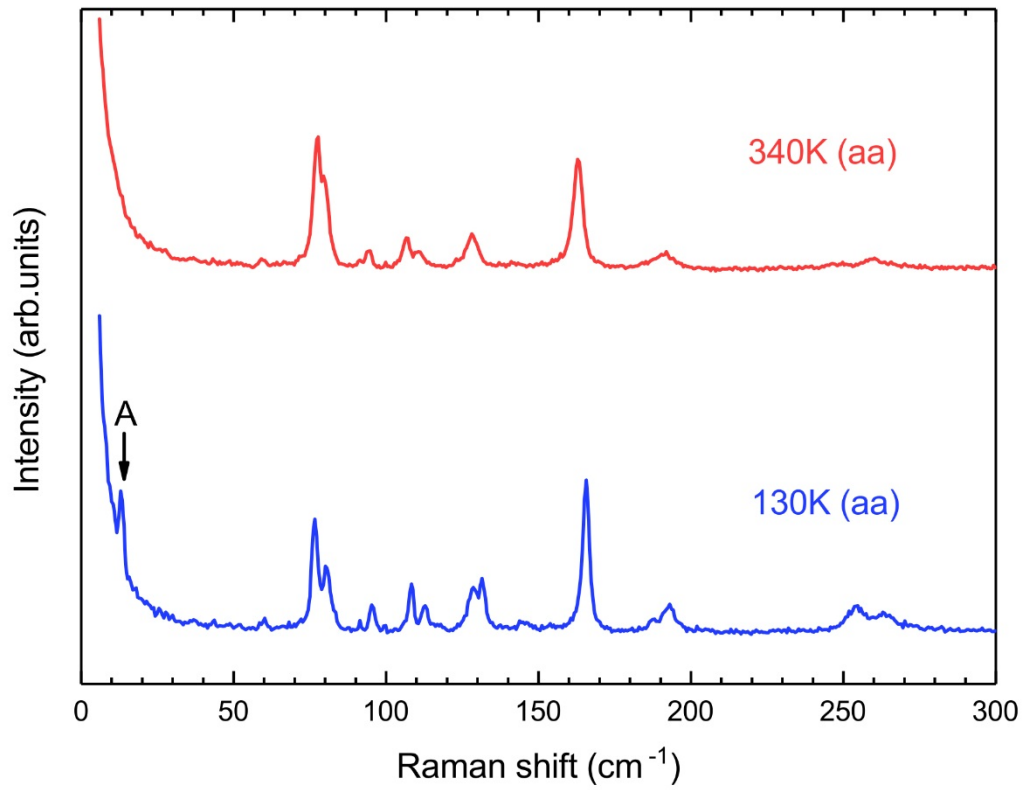


Fig.S5: **Full Raman spectra of few-layer MoTe₂.**

Polarized Raman spectra of a 22nm sample in aa configuration. The red curve was measured at 340K during cooling. A peak is unobservable and the sample stayed at $1T'$ phase. The blue curve was measured at 130K during cooling. The A peak emerged as the sample transformed to the T_d phase.